Error Model for Scene Reconstruction from Motion and Stereo

Songfan Yang[1], Bir Bhanu[1], Anastasios I. Mourikis[2]

1. Center for Research in Intelligent Systems, University of California, Riverside, CA 92521.
2. Department of Electrical Engineering, University of California, Riverside, CA 92521.
{syang, bhanu, mourikis}@ee.ucr.edu

Abstract

Scene reconstruction from motion and stereo are the two most popular methods for 3D range reconstruction. Because both techniques are affected by different types of errors, combining these two approaches to carry out 3D reconstruction seems natural. In this work, we present the initial results of our work towards the goal of analytically describing the performance of such a synergistic system. We consider the case in which points are viewed from two vantage points, and analytically model the uncertainty in the reconstruction of their 3D position. The uncertainty is expressed as a function of the points' location in the scene, as well as of the viewpoint change between the two images. The analysis is complemented by numerical results, which shed light on several interesting properties of the estimation accuracy.

1. Introduction

In 3D scene understanding, structure from motion and stereo are two widely used techniques for 3D reconstruction and range estimation. In both cases, when dealing with real images reconstruction errors are inevitable. In order to predict the performance of any method, an analysis of the properties of the errors is necessary. A number of factors affect the error in 3D reconstruction: camera and object motion, measurement noise, spatial quantization in the image coordinates [14], feature point matching [13], intrinsic camera calibration [11, 12], unmodeled camera distortions, as well as the numerical and statistical properties of the chosen reconstruction method [5, 8, 9]. In this work, we focus on the effects of measurement noise, and carry out an analysis for the cases of 3D reconstruction from camera motion and from stereo.

Our long-term goal is to carry out scene reconstruction based on combining camera motion and stereo sensing [2, 3, 4], and to theoretically characterize the performance of the resulting system. In order to guide the design of the integrated system, we here seek to analyze the performance of each of the two methods individually. This will allow us to use the integration of both motion and stereo cues to compensate the flaws of each individual method, and to obtain better accuracy. It is worth noting that a system combining motion and stereo depth cues employs two methods similar to those employed by humans for depth perception. Therefore understanding its performance may provide helpful insights into the way humans perceive depth.

In this work we consider the case in which points are viewed from two vantage points, and analytically model the uncertainty in the reconstruction of their 3D position. The uncertainty is expressed as a function of the points' location in the scene, as well as of the viewpoint change between the two images. The uncertainty is represented by the Cramer-Rao lower bound, which provides us with the highest achievable accuracy any estimator may attain in estimating the position of the point. In our analysis, we focus on the uncertainty due to the image measurement noise (e.g., due to the inaccuracies of a feature detection algorithm). In our derivations we consider that this noise is the only source of error, and thus the camera intrinsic parameters as well as feature correspondence are considered perfectly known.

In what follows, we first discuss the relationship of our analysis to existing work (Section 2), and subsequently present the problem formulation for analytically computing the point reconstruction uncertainty in Section 3. This analysis is first carried out for general camera configurations, and then the important special cases of motion along the optical axis, as well as of a stereo pair of cameras are examined. Numerical results are demonstrated in Section 4.

2. Related Work and Our Contribution

A significant number of approaches have examined, in different contexts, the accuracy of structure and/or motion estimation. Most commonly, the problem being examined is that of Structure from Motion (SfM), in which both the camera motion and the scene structure are unknown (see, for example [14, 16] and references therein). In our work, we consider the problem where only the scene points are being estimated. Moreover, much of the existing work presents only empirical, but not analytical, results. For

978-1-4244-7030-3/10/$26.00 ©2010 IEEE

instance, it is demonstrated by Bhanu et al. [1] that motion reconstruction suffers a large error in the vicinity of the focus of expansion (FOE) while stereo reconstruction is inaccurate at the edges of field-of-view (FOV). Although numerical experimental evidence has shown that this statement holds true, the closed-form solution has not been given.

In order to obtain analytical results, in existing work often an approximate estimation algorithm is adopted, and then its accuracy is computed (e.g., [6, 7, 8, 10]). While this makes the derivations simpler, the use of a suboptimal algorithm is a limitation, due to the incurred loss of accuracy. Moreover, the resulting analysis is algorithm-specific. Finally, the prior work in the area of error modeling typically employs the continuous-time (optical flow) problem formulation (e.g. [14, 16]). While this may be reasonable for small camera motions, it is unclear whether the continuous-time formulation is applicable in the case of large baseline.

In this work, we compute the Cramer-Rao lower bound for the estimation of scene points, as a function of the camera viewpoint change and the points' location. The Cramer-Rao lower bound is a theoretical performance limit, and thus the results are algorithm-independent. In other words, different algorithms may introduce various errors in 3D reconstruction, but the error modeled here cannot be eliminated. Our analysis employs a "discrete" model (i.e., we consider perspective measurements in two images, instead of optic flow measurements), which makes the analysis applicable both to small- and large-baseline problems. Finally, we present numerical results that help visualize the estimation performance, for important cases of interest.

3. Technical Approach

In our work we consider the case where a feature point is observed from two different camera positions (either one moving camera, or a pair of cameras observing the point). In our error modeling process, we make several assumptions. (a) The cameras are well calibrated so that systematic errors are negligible. (b) Feature correspondences are error-free. (c) The relative configuration between the camera poses (rotation and translation) is perfectly known (d) The only source of error is the image measurement noise, which is modeled as a zero-mean random variable with Gaussian distribution. With these assumptions, we will analytically compute the Cramer-Rao bound for the 3D point's position estimation. The notation adopted in the following derivations is summarized in Table 1.

3.1. Evaluation of the Cramer-Rao Lower Bound

The camera observations are modeled by the perspective camera model, as shown in Figure 1. The

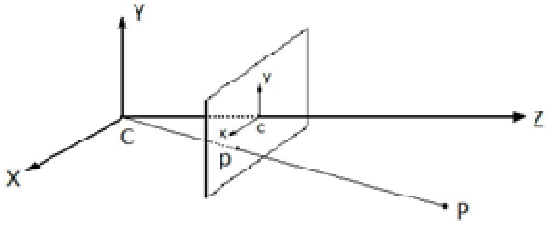

Figure 1: Ideal perspective camera model. C denotes the camera coordinates origin, and c represents the principal point on the ideal image plane. P is the 3D point in camera coordinates, and p is the projection of P on the image plane.

Variable	Meaning
$(X,Y,Z)^T$	points in world coordinates
$(u,v,w)^T$	points in homogeneous normalized image coordinates
$(x,y)^T$	points in normalized image coordinates
n, n'	Gaussian noise vectors
$\sigma^2 \boldsymbol{I}_{2\times 2}$	Covariance matrix of Gaussian noise
ω	Stacked noise vector
M	Stacked measurement vector
$\Lambda_M(P)$	Likelihood function
$h(P)$	Non-linear measurement function
H	Jacobian of $h(P)$ with respect to P
R	distance from the feature point to the origin
Q	Parameter vector $Q = \left[\frac{X}{Z} \quad \frac{Y}{Z} \quad R\right]^T$
A	Jacobian of Q with respect to P
Σ_P	covariance of the estimated P
Σ_Q	covariance of the estimated Q

Table 1: Variables used in derivation

mapping from the point with 3D world coordinates $P = (X,Y,Z)^T$ to the homogeneous normalized camera coordinates $p = (u,v,w)^T$ is given by

$$\begin{bmatrix} u \\ v \\ w \end{bmatrix} = [\boldsymbol{R} \quad \boldsymbol{T}] \begin{bmatrix} X \\ Y \\ Z \\ 1 \end{bmatrix} \tag{1}$$

where $\boldsymbol{R}$ is the 3×3 rotation matrix from the world frame to the camera frame, and $\boldsymbol{T}$ is the translation vector from the origin of the camera frame to origin of the world frame. The corresponding point on the normalized image plane is given by

$$\begin{bmatrix} x \\ y \end{bmatrix} = \begin{bmatrix} \frac{u}{w} \\ \frac{v}{w} \end{bmatrix} \tag{2}$$

To simplify the derivations, we assume that the world frame coincides with the first camera frame, which results in $R_1 = \boldsymbol{I}$, $T_1 = 0$. Then, the world point projection on the first image, p_1, is given by:

$$m_1 = \begin{bmatrix} \frac{u}{w} \\ \frac{v}{w} \end{bmatrix} + n = \begin{bmatrix} \frac{X}{Z} \\ \frac{Y}{Z} \end{bmatrix} + n \quad (3)$$

Here n is the measurement noise, assumed to be a zero-mean Gaussian vector with variance σ^2 in each direction: $n \sim \mathcal{N}(0, \sigma^2 \boldsymbol{I}_{2\times 2})$.

We denote the camera rotation and translation in the second time instant by $R = [r_1^T \quad r_2^T \quad r_3^T]^T$, $T = [t_1 \quad t_2 \quad t_3]^T$. Then the measurement of the point P in image 2, denoted p_2, is given by:

$$m_2 = \begin{bmatrix} \frac{r_1^T P + t_1}{r_3^T P + t_3} \\ \frac{r_2^T P + t_2}{r_3^T P + t_3} \end{bmatrix} + n' \quad (4)$$

Where similarly, $n' \sim \mathcal{N}(0, \sigma^2 \boldsymbol{I}_{2\times 2})$ is the measurement noise, which is independent from n.

p_1 and p_2 are the two measurements available for computing the position of the point P. We stack these two measurements in a single vector, to obtain the measurement equation:

$$M = \begin{bmatrix} m_1 \\ m_2 \end{bmatrix} = \begin{bmatrix} \frac{X}{Z} \\ \frac{Y}{Z} \\ \frac{r_1^T P + t_1}{r_3^T P + t_3} \\ \frac{r_2^T P + t_2}{r_3^T P + t_3} \end{bmatrix} + \begin{bmatrix} n_{11} \\ n_{22} \\ n'_{11} \\ n'_{22} \end{bmatrix} \quad (5)$$

Which is of the general form

$$M = h(P) + \omega \quad (6)$$

Where

$$h(P) = \begin{bmatrix} \frac{X}{Z} & \frac{Y}{Z} & \frac{r_1^T P + t_1}{r_3^T P + t_3} & \frac{r_2^T P + t_2}{r_3^T P + t_3} \end{bmatrix}^T$$

and the measurement noise vector is $\omega \sim \mathcal{N}(0, \sigma^2 \boldsymbol{I}_{4\times 4})$.

Our goal is to estimate the parameter vector $(X, Y, Z)^T$ based on the measurements of M. For this purpose we employ the maximum-likelihood estimation paradigm, which requires the maximization of the likelihood function given by

$$\Lambda_M(P) = p(M; P) \quad (7)$$

In practice we can carry out this maximization either analytically (in special cases) or by employing a nonlinear optimization algorithm such as the Gauss-Newton method. However, here we are not interested in the implementation aspect of the problem, but rather in the analytical evaluation of the estimation performance. This can be carried out by computing the Cramer-Rao bound, which provides us the best possible estimation accuracy attainable. It should be pointed out that this bound is typically not a loose one, and if an estimator that attains this bound exists, this will be the Maximum Likelihood estimator [17].

The Cramer-Rao bound provides us with the covariance matrix of the best possible estimator. This is given by:

$$\Sigma_P = \sigma^2 (H^T H)^{-1} \quad (8)$$

where $H = \frac{\partial h}{\partial P}$ is the Jacobian of $h(P)$ with respect to P. This matrix is the covariance matrix of the estimation errors in the parameter vector $(X, Y, Z)^T$. However, we are interested in examining the range estimation accuracy. For this reason, we define a different parameterization for the feature position, in which the range, $R = \sqrt{X^2 + Y^2 + Z^2}$, appears explicitly. We denote this parameterization $Q = \begin{bmatrix} \frac{X}{Z} & \frac{Y}{Z} & R \end{bmatrix}^T$. Then, the Cramer-Rao bound for the covariance of the estimation error in Q is given by

$$\Sigma_Q = A \Sigma_P A^T \quad (9)$$

where $A = \partial Q / \partial P = \begin{bmatrix} \frac{1}{Z} & 0 & -\frac{X}{Z^2} \\ 0 & \frac{1}{Z} & -\frac{X}{Z^2} \\ \frac{X}{R} & \frac{Y}{R} & \frac{Z}{R} \end{bmatrix}$.

Equations (8) and (9) analytically describe the attainable accuracy in estimating the 3D position of a point in 3D. In the following sections, we will examine the structure and properties of this result in two special cases of interest.

3.2 Special Case: Camera Motion along the Optical Axis

A case of interest which arises often in practice is that of a single camera moving along its optical axis (e.g., a forward-looking camera on a robot). We here examine the accuracy of structure estimation in this case. In order to evaluate the closed-form solution, we further assume that the orientation of the camera remains the same in both time instants, and thus we only have translation along the Z axis ($t_1 = t_2 = 0$). In this case, we obtain

$$h_M(P) = \begin{bmatrix} \frac{X}{Z} & \frac{Y}{Z} & \frac{X}{Z+t_3} & \frac{Y}{Z+t_3} \end{bmatrix}^T \quad (10)$$

Which gives rise to a Jacobian with respect to $P = (X, Y, Z)^T$ equal to:

$$H_M = \begin{bmatrix} \frac{1}{Z} & 0 & -\frac{X}{Z^2} \\ 0 & \frac{1}{Z} & -\frac{Y}{Z^2} \\ \frac{1}{Z+t_3} & 0 & -\frac{X}{(Z+t_3)^2} \\ 0 & \frac{1}{Z+t_3} & -\frac{X}{(Z+t_3)^2} \end{bmatrix} \quad (11)$$

Substituting this result in Eq. (9) we can obtain the Cramer-Rao bound for the parameter vector Q. We are especially interested in the accuracy with which the range, *R*, can be estimated. The standard deviation of the range estimation errors is given by the square root of the (3,3) element of the covariance matrix in Eq. (9), which is calculated as

$$U_M = \frac{\sigma}{t_3 R}\sqrt{\frac{N}{(X^2+Y^2)}} \quad (12)$$

where
$N = 2X^4Z^4 + 4X^4Z^3t_3 + 6X^4Z^2{t_3}^2 + 4X^4Z{t_3}^2 + X^4{t_3}^4 + 4X^2Y^2Z^4 + 8X^2Y^2Z^3t_3 + 12X^2Y^2Z^2{t_3}^2 + 8X^2Y^2Z{t_3}^3 + 2X^2Y^2{t_3}^4 + 4X^2Z^6 + 10X^2Z^5t_3 + 12X^2Z^4{t_3}^2 + 8X^2Z^3{t_3}^3 + 2X^2Z^2{t_3}^4 + 2Y^4Z^4 + 4Y^4Z^3t_3 + 6Y^4Z^2{t_3}^2 + 4Y^4Z^2{t_3}^2 + 2Y^4{t_3}^4 + 4Y^2Z^6 + 10Y^2Z^5t_3 + 12Y^2Z^4{t_3}^2 + 8Y^2Z^3{t_3}^3 + 2Y^2Z^2{t_3}^4 + 2Z^8 + 6Z^7t_3 + 7Z^6{t_3}^2 + 4Z^5{t_3}^2 + Z^4{t_3}^4.$

3.2.1 Discussion

Equation (12) describes the range estimation uncertainty, in the case of forward camera motion, as a function of the feature position and the translation amount, t_3. Several observations can then be obtained.

(a) $U_M = \infty$ when $t_3 = 0$. This is reasonable because without translation, the images obtained at two time instances are the same, and the 3D structure cannot be reconstructed.

(b) $U_M = \infty$ when $X = Y = 0$. This occurs because the 3D point is along the FOE, and thus it is projected to the same image point on consecutive images. As a result, no 3D information is available.

(c) The uncertainty value is symmetric with respect to both the X axis and Y axis.

(d) In many practical situations, the point's Z coordinate will be larger than the X and Y coordinates, as well as larger than the translation, t_3. In this case, the Z^8 term dominates the numerator and as t_3 increases, the value of uncertainty will decrease. This effect is shown in the experimental results.

3.3 Uncertainty from Stereo

A second case of practical interest is the one in which the point is concurrently observed by two cameras in a stereo-pair configuration (see Figure 2). In this case, the rotation matrix between the two cameras is the identity matrix, and the translation lies along the x axis only. If we denote the baseline between the two cameras as b, then the measurement function becomes:

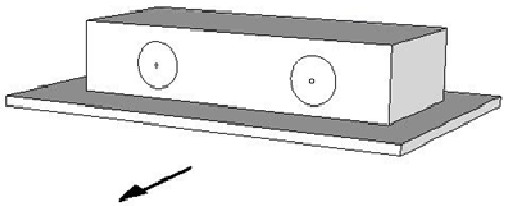

Figure 2: Stereo camera system. A pair of identical cameras is built inside the stereo camera shell.

$$h_S(P) = \begin{bmatrix} \frac{X}{Z} & \frac{Y}{Z} & \frac{X+b}{Z} & \frac{Y}{Z} \end{bmatrix}^T \quad (13)$$

and its Jacobian with respect to *P* is

$$H_S = \begin{bmatrix} \frac{1}{Z} & 0 & -\frac{X}{Z^2} \\ 0 & \frac{1}{Z} & -\frac{Y}{Z^2} \\ \frac{1}{Z} & 0 & -\frac{X+b}{Z^2} \\ 0 & \frac{1}{Z} & -\frac{X}{Z^2} \end{bmatrix} \quad (14)$$

The standard deviation of the range estimation errors in this case is given by:

$$U_S = \frac{\sigma Z}{bR}\sqrt{\frac{N}{2}} \quad (15)$$

where
$N = 4X^4 + 4X^3b + 8X^2Y^2 + 8X^2Z^2 + 2X^2b^2 + 4XY^2b + 4XZ^2b + 4Y^4 + 8Y^2Z^2 + Y^2b^2 + 4Z^4.$

3.2.2. Discussion

Several observations can also be made from eq. (15).

(a) In contrast to the previous case of forward motion, the uncertainty value reaches the lowest value at the center of the ideal image plane.

(b) The uncertainty value is symmetrical about neither the X axis nor the Y axis. This is because we derive the equation with respect to the left camera, not the center of the stereo pair.

(c) The uncertainty is decreasing as b becomes larger.

(d) For large Z (i.e., as the feature moves away from the camera), the uncertainty increases approximately proportionally to Z^2.

4. Experimental Results

We carry out experiments by modeling a stereo pair of cameras with the same intrinsic parameters. While the platform is moving, both of the cameras are taking pictures, and we carry out reconstruction by either considering the images of the left camera only, or by considering the measurements of the two stereo cameras at the first instance only. Table 2 contains the simulation parameters.

Variable	Meaning	Value
f	Focal length	6.6e-3 m
L	Image plane length	1024 pixel
W	Image plane width	768 pixel
σ	Measurement variance	7.1023e-4m
f_x	Intrinsic parameter	2.1333e5
f_y	Intrinsic parameter	2.1333e5
t_3	Translation along Z axis	1m
b	Baseline	0.12m

Table 2: Simulation parameter values

4.1. Uncertainty of Reconstruction from Forward Camera Motion

Results for this special case of the motion-based scene reconstruction, discussed in Section 3.2.1, are shown in Figures 3 to 8. First, we set $Z = 40m$, $t_3 = 1m$, and calculate the range error uncertainty by use of eq. (12). Figure 3 shows the 2D view of the result on the 1024×768 image plane. Figure 4 is a zoomed-in version of Figure 3, showing only an 80×80 pixel area around the center of the image, Figure 5 is the 3D surface plot of the result, while Figure 6 shows a number of "slices" of the surface plot, taken every 20 pixels along the Y axis. Note that, as discussed earlier, the uncertainty is infinite at the principal point of the image. Thus, we have defined a small "blind

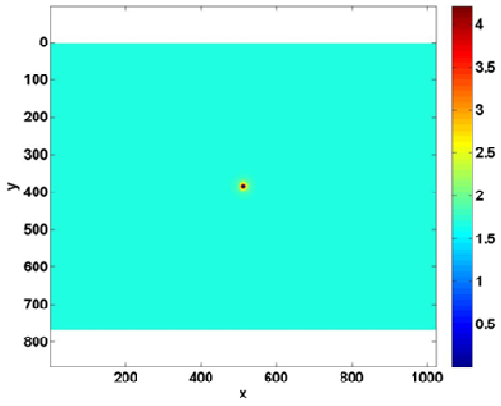

Figure 3: Forward motion: 2D view of the range reconstruction uncertainty. It is calculated by Eq. (12) with the following parameter values. $Z = 40m$, $t_3 = 1m$.

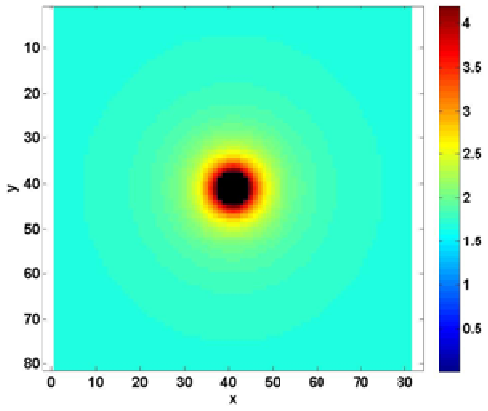

Figure 4: Forward motion: The center view of the range reconstruction uncertainty. It is calculated by eq. (14) with the following parameter values. $Z = 40m$, $t_3 = 1m$. The black area is the "blind region".

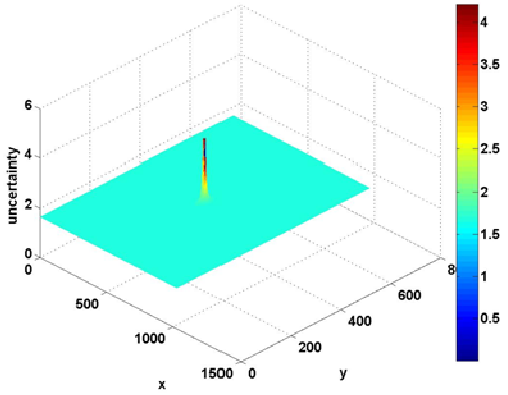

Figure 5: Forward motion: 3D view of the range reconstruction uncertainty. It is calculated by eq. (14) with the following parameter values. $Z = 40\text{m}$, $t_3 = 1\text{m}$.

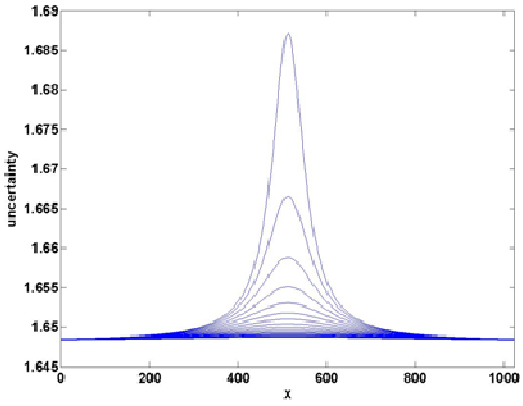

Figure 6: Forward motion: Slice of the 3D view of the range reconstruction uncertainty. (Excluding immediate vicinity of FOE) The slices of the 3D shape along X axis are taken every 20 pixels of the Y axis.

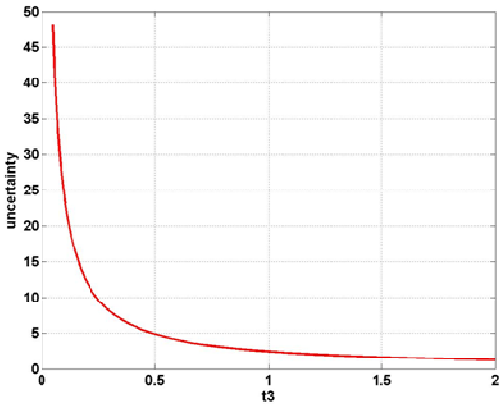

Figure 7: Forward motion: Change of the range reconstruction uncertainty with respect to t_3. It is calculated by Eq. (12) with the following parameter values. $X = 20m, Y = 30m, Z = 40m.$

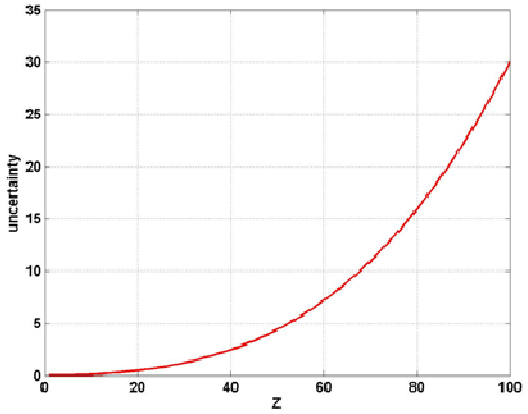

Figure 8: Forward motion: Change of the range reconstruction uncertainty with respect to Z. It is calculated by Eq. (12) with following parameter value. $X = 20m, Y = 30m, t_3 = 1m.$

region" around the image center where the results are not plotted, to maintain the clarity of the figure in the remaining areas.

These plots demonstrate that, as expected, the uncertainty is maximum close to the FOE, and sharply decreases away from it. Even though this may be unclear from the color-coded Figures 3-5, we point out that the uncertainty value in the region other than the image center is not constant. It is constantly decreasing as we move away from the FOE, as shown in Figure 6.

We next analyze the behavior of the range reconstruction uncertainty with respect to t_3. As discussed in Section 3.2.1, as t_3 increases, the value of uncertainty will decrease. This is demonstrated in Figure 7, where the parameters $X = 20m, Y = 30m, Z = 40m$ have been used.

Finally, we consider the change of the range reconstruction uncertainty with respect to Z. This is demonstrated in Figure 8, where the parameters X = 20m, Y = 30m, t_3 = 1m have been used. This plot corroborates the findings discussed in Section 3.2.1.

4.2. Uncertainty of Stereo-based Scene Reconstruction

Results for the special case of the stereo reconstruction are shown in Figures 9 to 13. First, we examine the behavior of the uncertainty on the image plane. For this purpose, we set $Z = 10m$, b = 0.12m, and calculate the uncertainty value using Eq. (15). Figures 9 and 10 show the results both as a 2D plot on the image plane, and as a 3D surface plot. Note that, in contrast to the case of forward motion, the uncertainty is larger towards the end of the image.

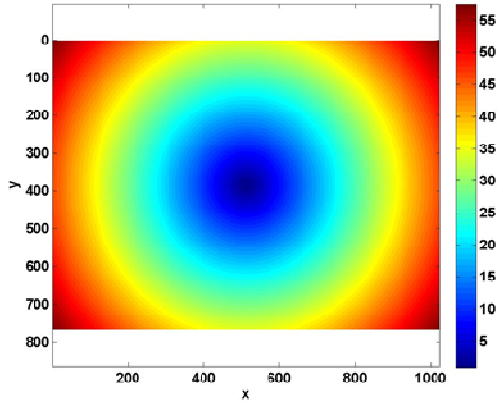

Figure 9: Stereo reconstruction: 2D view of the range uncertainty. It is calculated by eq. (15) with the following parameter values. $Z = 10m, b = 0.12m.$

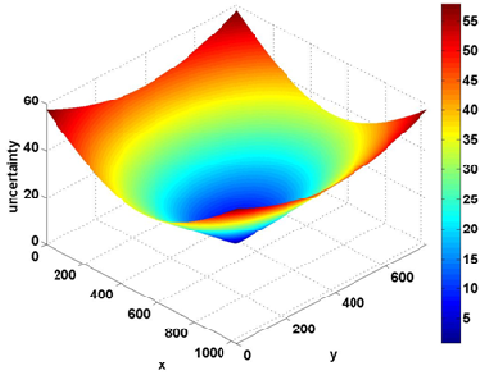

Figure 10: Stereo reconstruction: 3D view of the range uncertainty. It is calculated by eq. (15) with the following parameter values. $Z = 10m$, $b = 0.12m.$

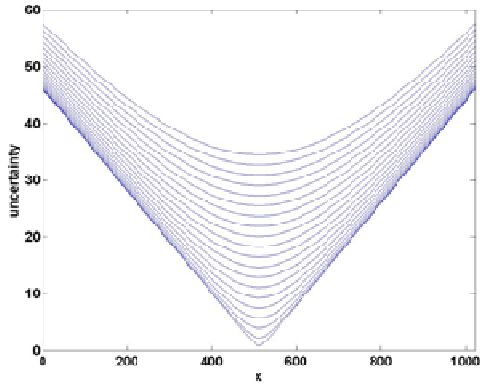

Figure 11: Stereo reconstruction: Slice of the 3D view of the range reconstruction uncertainty. The slices of the 3D shape along X axis are taken every 20 pixels of Y axis.

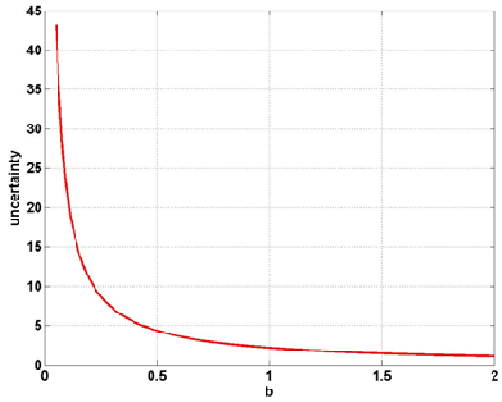

Figure 12: Stereo reconstruction: Change of the range uncertainty with respect to b. It is calculated by Eq. (15) with the following parameter values. $X = 20m, Y = 30m, Z = 10m$.

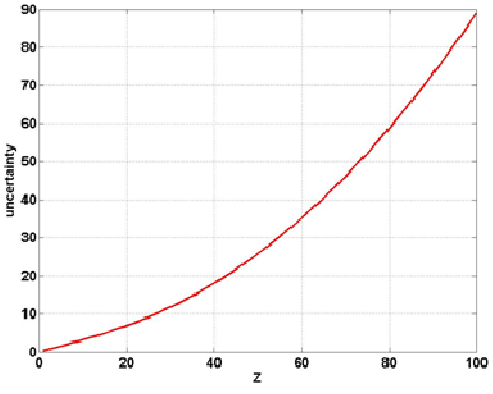

Figure 13: Stereo reconstruction: Change of the range uncertainty with respect to Z. It is calculated by Eq. (15) with the following parameter values. $X = 20m, Y = 30m, b = 0.12m$.

Figure 12 demonstrates the change of the range uncertainty with respect to b, which approximately follows a 1/b curve. For this plot, we used $X = 20m, Y = 30m, Z = 10m$. Finally, Figure 13 shows the change of the range uncertainty with respect to Z. For this plot, we used $X = 20m, Y = 30m, b = 0.12m$.

5. Conclusions

Error modeling for both motion-based and stereo-based reconstruction is an important topic. In this paper, we have analytically computed the Cramer-Rao bound for two-view reconstruction, and explored the properties of the estimation uncertainty for the important special cases of forward camera motion and stereo-based reconstruction. Our analysis addresses both problems in a unified framework, and allows for the derivation of closed-form results. A number of key observations were made, which will be instrumental in designing a system that uses both motion and stereo information for scene reconstruction. Most importantly, we observed that in forward-motion based reconstruction, the uncertainty of points along FOE (the center of the image) tends to approach infinity. In contrast, for stereo-based reconstruction, the uncertainty is worse close to the image borders. This suggests that stereo-based and forward-motion-based depth cues are in a sense complementary. This could be leveraged in designing systems that utilize both types of cues simultaneously.

In our future work, we will use the analysis presented here as a stepping stone towards modeling more system characteristics, and examining their impact on accuracy. These include the errors of calibration, motion estimation, correspondence, etc. The end goal of this work is to predict the performance of a synergistic motion/stereo system, under real-world circumstances.

Acknowledgement: This work is partially supported by NSF grants 0915270 and 0727129.

References

[1] B. Bhanu, P. Symosek, S. Snyder, B. Roberts, and S. Das, Synergism of Binocular and Motion Stereo for Passive Ranging. *IEEE Transactions on Aerospace and Electronic Systems*, vol. 30, issue 3, pp: 709-721,1994.

[2] C. Strecha, and L. V. Gool. Motion - Stereo Integration for Depth Estimation. *European Conference on Computer Vision*, LNCS 2351, pp: 170-185, 2002.

[3] B. Bhanu, S. Das, B. Roberts, and D. Duncan. A System for Obstacle Detection during Rotorcraft Low Altitude Flight. *IEEE Transactions on Aerospace and Electronic Systems*, vol. 32, issue 3, pp: 875-897, 1996.

[4] P.K. Ho, and R. Chung. Stereo-Motion with Stereo and Motion in Complement. *Journal of Pattern Recognition and Machine Intelligence*, vol. 22, issue 2, pp: 215-220, 2000

[5] J. Oliensis. A New Structure from Motion Ambiguity. *IEEE Transaction on Pattern Analysis and Machine Intelligence*, vol. 22, issue 7, pp: 685-700, 2000.

[6] J. Weng, T. Huang, and N. Ahuja. Error Analysis of Motion Parameter Estimation from Image Sequences. *International Conference on Computer Vision*, pp: 703-707, 1987.
[7] W. Sohn, N.D. Kehtarnavaz. Analysis of Camera Movement Errors in Vision-Based Vehicle Tracking. *IEEE Transaction on Pattern Analysis and Machine Intelligence*, vol. 17, issue 1, pp: 57-61, 1995.
[8] E.J. Weldon, Jr., H. Liu. How Accurately Can Direct Motion Vision Determine Depth. *IEEE Conference on Computer Vision and Pattern Recognition*, pp: 613-618, 1991.
[9] J. Thomas, A. Hanson, and J. Oliensis. Understanding Noise: The Critical Role of Motion Error in Scene Reconstruction. *International Conference on Computer Vision*, pp: 325-329, 1993.
[10] L. Matthies, S. Shafer. Error Modeling in Stereo Navigation. *IEEE Transaction on Robotics and Automation*, vol. 3, issue 3, pp: 239-248, 1987.
[11] L.F. Cheong, and C.H. Peh. Depth Distortion Under Calibration Uncertainty. *Computer Vision and Image Understanding*, vol. 93, No. 3, pp: 221-244, 2004.
[12] M. Zucchelli, and J. Kosecka. Motion Bias and Structure Distortion Induced by Intrinsic Calibration Errors. *Image and Vision Computing*, vol. 26, No. 5, pp: 639-646, 2008.
[13] R. Mayoral, G. Lera, and M.J. Pérez-Ilzarbe. Evaluation of Correspondence Errors for Stereo. *Image and Vision Computing* , vol. 24, No. 12, pp: 1288-1300, 2006.
[14] J. Weng, T. Huang, and N. Ahuja. Motion and Structure from Two Perspective Views: Algorithms, Error Analysis, and Error Estimation. *IEEE Transaction on Pattern Analysis and Machine Intelligence*, vol. 11, issue 5, pp: 451-476, 1989.
[15] J. Nocedal, S. Wright. Numerical optimization. New York: Springer. ISBN 0387987932, 1999.
[16] A.K. Roy-Chowdhury, R. Chellappa. Robust Estimation of Depth and Motion Using Stochastic Approximation. *International Conference on Computer Vision*, pp: 642-645, 2001.
[17] S. M. Kay. Fundamentals of Statistical Signal Processing: Estimation Theory. Englewood Cliffs, NJ: Prentice-Hall, 1993.